MATERIALS CHEMISTRY
FRONTIERS

Accepted Manuscript

This article can be cited before page numbers have been issued, to do this please use: Z. Xu, J. Lin, L. Zhang, X. Tian and L. Wang, *Mater. Chem. Front.*, 2019, DOI: 10.1039/C9QM00366E.

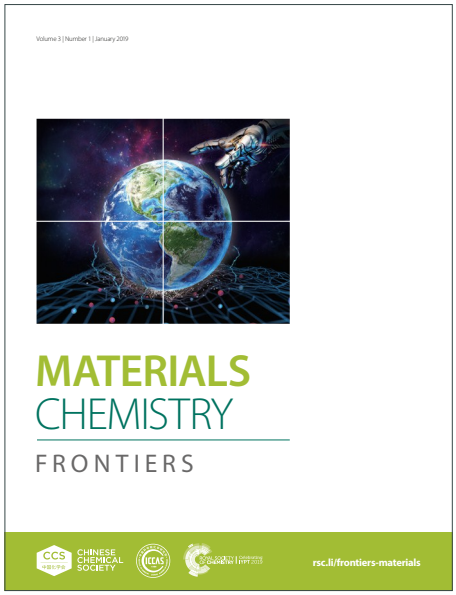

View Article Online
DOI: 10.1039/C9QM00366E

ARTICLE

Modulation of Molecular Orientation Enabling High Photovoltaic Performance of Block Copolymer Nanostructures†

Received 00th January 20xx,
Accepted 00th January 20xx

DOI: 10.1039/x0xx00000x

Zhanwen Xu, Jiaping Lin,* Liangshun Zhang, Xiaohui Tian and Liquan Wang*

Block copolymer self-assembly is a promising strategy for high-performance polymer solar cells. However, the power conversion efficiencies of block-copolymer-based solar cells are still not as high as expected. Herein, by means of theoretical simulations we show a distinct improvement in the photovoltaic performance of donor-acceptor block copolymer thin films *via* regulating molecular orientation. Self-assembled lamellae perpendicular to the electrodes with modulated molecular orientation were obtained by applying electric fields during the block copolymer self-assembly. Our theoretical calculations indicate that compared with the general ones without external field treatment, the power conversion efficiencies of the block copolymer nanostructures with modulated molecular orientation can be improved by more than 150% with high values of short current densities and fill factors. The improvement in the photovoltaic performance is ascribed to the simultaneous enhancement in exciton diffusion to donor/acceptor interfaces and charge carrier transport to electrodes. Our findings could yield guidelines for the design of photovoltaic materials with improved photovoltaic performance *via* control over the molecular orientation.

1 Introduction

Polymer solar cells (PSCs), offering advantages such as low cost, high mechanical flexibility, light weight and large-area manufacturing compatibility at relatively low processing temperatures, have received increasing attention.[1, 2] The performance of polymer solar cells has been greatly improved since the introduction of bulk heterojunctions (BHJ) for the active layer.[3-5] Recently, many research have been conducted on BHJ PSCs with nonfullerene acceptors, and power conversion efficiencies (PCEs) up to 14% for single-junction solar cells and 17% for tandem solar cells were achieved.[6-8] However, the efficiencies required to compete in the energy market have not yet been realized. Notably, block-copolymer-based polymer solar cells, which are very promising, have not yet shown efficiencies that are high as expected.[9-14] Enhancing the photovoltaic performance of polymer solar cells presents a pressing challenge.

High photovoltaic performance in PSCs requires optimization of photovoltaic processes, including light absorption, exciton dissociation (charge carrier generation) at the donor/acceptor (D/A) interface, and transport and collection of the charge carriers.[2, 15] These photovoltaic processes are strongly dependent on structural characteristics such as domain size, domain purity, interfacial area and crystal structures.[16-18] Among these characteristics, the molecular orientation has also been shown to affect the performance of polymer photovoltaics, which results from the anisotropic transport of excitons and charge carriers in semiconducting polymers.[16, 19-25] It was reported that molecular orientation in polymer blend solar cells can be tuned through optimization of processing conditions including choice of solvents, thermal treatment and external field treatment, or through chemical strategies.[24, 26-29] However, in polymer blend systems, modulation of the alignment of molecules is inevitably associated with changes in blend nanostructures, such as domain size and phase purity.[19] In contrast, block copolymers can self-assemble into highly ordered and controllable nanostructures, which can be used to prepare highly efficient PSCs.[10, 13, 30] However, for block-copolymer-based solar cells, precise modulation and positive effects of molecular orientation are rarely acknowledged. The modulation and effects of molecular orientation on the performance of block-copolymer-based solar cells should be systematically studied to level up the efficiency, which could be facilitated by model construction and theoretical simulations.

Theoretical simulations have been used to analyze the relationship between the nanostructures and the photovoltaic properties of complex polymer systems.[31-38] For example, Buxton et al. developed a drift-diffusion model for polymer solar cells and combined it with the Cahn-Hilliard model to study the effect of the morphologies formed by diblock copolymers on photovoltaic performance.[31, 39] Their results indicated that the performance of the diblock copolymers can

Shanghai Key Laboratory of Advanced Polymeric Materials, State Key Laboratory of Bioreactor Engineering, Key Laboratory for Ultrafine Materials of Ministry of Education, School of Materials Science and Engineering, East China University of Science and Technology, Shanghai 200237, China. E-mail: jlin@ecust.edu.cn, lq_wang@ecust.edu.cn

† Electronic supplementary information (ESI) available. See DOI:

View Article Online
DOI: 10.1039/C9QM00366E

be improved by forming ordered structures. Recently, we proposed a multi-scale approach coupling dissipative particle dynamics (DPD) with a drift-diffusion model to study the photovoltaic properties of donor-acceptor multiblock copolymers.[34] Information on the molecular packing of the complex block copolymers in the nanostructures can be easily obtained through DPD simulations. It was found that modulating the nanostructures via molecular design is an effective way to improve the photovoltaic performance of block copolymers. However, the effect of molecular orientation, which is crucial for determining the photovoltaic performance, has not been considered in the previous studies. Herein, we extend the multi-scale approach to include the effect of molecular orientation on the photovoltaic performance of block copolymer thin films. In the extended approach, the anisotropic characteristics of the mobility of excitons and charge carriers are considered, given that the mobility can be varied significantly by modulating the orientation of the polymer chains.[21, 40]

In this work, we applied the extended multi-scale approach to investigate the effect of the molecular orientation on the photovoltaic performance of donor-acceptor (DA) diblock copolymer thin films. To the best of our knowledge, we report the first investigation of improving the photovoltaic performance of block copolymer thin films via modulating molecular orientation. The molecular orientation in diblock copolymer thin films was modulated through external field treatment. The calculations on photovoltaic properties demonstrate that the photovoltaic performance of the block copolymer thin films can be significantly improved when the molecular orientation is optimized. We expect this work to provide useful information for designing advanced photovoltaic materials based on block copolymers.

2 Results and Discussion

Molecular orientation markedly influences photovoltaic performance of the PSCs. To incorporate the effect of molecular orientation into the theoretical simulations, we introduced an external electric field into the DPD simulations to modulate the molecular orientation and considered the anisotropic transport of excitons and charge carriers in the drift-diffusion model. In the DPD simulations, we constructed a coarse-grained model of donor-acceptor block copolymers (D_4A_4) confined between two parallel substrates, as characteristically shown in Figure 1. The photovoltaic performance of DA diblock copolymers with different molecular weights, such as D_5A_5 and D_6A_6, was also examined, and the findings in this work are general to a broad range of block copolymers with various molecular weights. The top and bottom plates, corresponding to the anode and cathode respectively, are modeled by a set of fixed substrate particles that are placed at the lattice points of the FCC crystal in three layers. An electric field treatment was applied during the self-assembly of the donor-acceptor diblock copolymers. The interaction between the block copolymers and the external electric field is modeled by coupling the unit vector **P**

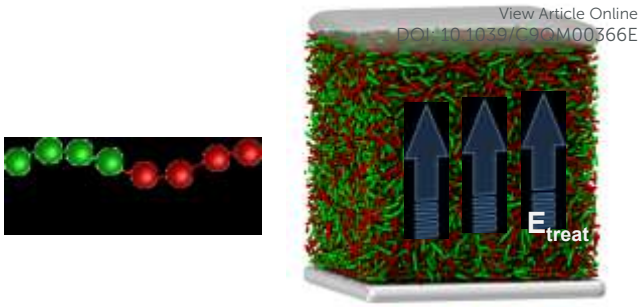

Figure 1 DPD model of the donor-acceptor diblock copolymers confined in thin films with electric-field treatment during the self-assembly process. The green and red colors are assigned to donor and acceptor particles in the copolymers, respectively.

along the long axis of the donor blocks to the external field $\mathbf{E}_{treat}$.

The photovoltaic performance of the self-assembled nanostructures was obtained by solving the extended drift-diffusion equations. In the extended formalism, the anisotropy of the mobility is determined by the order parameter and inherent anisotropic characteristic of the block copolymers. The anisotropic characteristic of the block copolymers is described by the anisotropic transport characteristic parameter (C_A), which is defined as the ratio of the mobility $\mu_{||}$ along the backbone of block copolymers to the mobility $\mu_{\perp}$ perpendicular to the backbone. Details about drift-diffusion theory, such as the choices of parameters, can be found in Section 2 of the Supporting Information.

2.1 Enhanced Photovoltaic Performance of Self-Assembled Nanostructures with Modulated Molecular Orientation

In this subsection, the effect of the molecular orientation on the photovoltaic performance in thin films of DA diblock copolymers was examined. An external field was applied to manipulate the molecular orientation of the block copolymers in the thin films. The electrodes were set to be neutral to both the donor and acceptor blocks, and thus they do not prefer the either block. The thickness was set to $4l_0$, where l_0 is the period of the lamellae of the DA diblock copolymers without external field treament.

To obtain block copolymer nanostructures with different molecular orientations, we applied various external treated fields with different values and orientations during the self-assembly processes. Figure 2a-c show the three-dimensional structures of the DA block copolymer films with and without external field treatment during the self-assembly process. In all the self-assembled nanostructures, the domains are perpendicular to the electrodes. From the 3-dimensional views of the nanostructures, one can identify that the external field has a significant effect on the molecular orientation of the block copolymers. As shown in Figure 2a, when no external field is applied during the self-assembly process, the diblock copolymers form nanostructures with most of the donor and

acceptor blocks perpendicular to the D/A interfaces (see Figure 2a). When the external field is applied upward, the free ends of the donor and acceptor blocks point towards the anode and cathode, respectively (see Figure 2b). When the external field is applied downward, the free ends of the donor and acceptor blocks in the self-assembled nanostructures point towards the cathode and anode, respectively (see Figure 2c).

To gain further insight into the effect of external field treatment on the self-assembled nanostructures, the molecular orientation of the block copolymers, domain size and interface width were characterized. We used the orientation angle (θ) and order parameter (*S*) to quantitatively describe the molecular orientation. The orientation angle is defined as the angle between the donor block and the vector perpendicular to the electrodes (see Figure 2d). The average values of the angle (<θ>) are calculated and plotted in Figure 2e. The <θ> changes markedly within the $\mathbf{E_{treat}}$ range from -10 to 10 (the negative and positive values of $\mathbf{E_{treat}}$ indicate that the external field is applied downward and upward respectively). When the $\mathbf{E_{treat}}$ is 0, the <θ> is 90°, which indicates that most of the block copolymers are perpendicular to the D/A interfaces. In the two nanostructures treated with negative and positive $\mathbf{E_{treat}}$, the <θ> changes slightly when $|\mathbf{E_{treat}}|$ is larger than 10**.** The external field treatment can also affect the orientation order of the block copolymers (see Figure 2e). The order parameters in these structures increase steadily wit increasing $|\mathbf{E_{treat}}|$. Compared with the molecular orientation, the domain size and interface width show less sensitivity to the variation in the $\mathbf{E_{treat}}$ under the present conditions employed, as shown in Figure 2f.

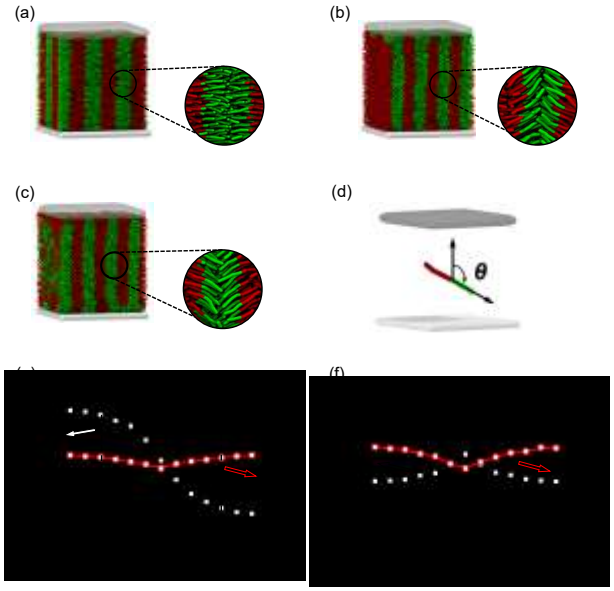

Figure 2 (a)-(c) Nanostructures self-assembled from donor-acceptor diblock copolymers with and without external field treatment during the self-assembly process. (a) $\mathbf{E_{treat}}$=0, (b) $\mathbf{E_{treat}}$=10 and (c) $\mathbf{E_{treat}}$=-10 (**SPE**, **SDA** and **SDC** are formed respectively). The negative and positive values of $\mathbf{E_{treat}}$ indicate that the external field is applied downward and upward respectively. (d) The illustration for the definition of the angle θ between the donor block and the vector normal to the D/A interfaces. (e) Plots of the average value of the angle (<θ>) and the order parameter (*S*) against $\mathbf{E_{treat}}$. (f) Plots of the domain width and interfacial width against $\mathbf{E_{treat}}$.

The effect of molecular orientation on the photovoltaic performance was then examined. We took the nanostructures treated with $\mathbf{E_{treat}}$=0, $\mathbf{E_{treat}}$=-10 and $\mathbf{E_{treat}}$=10 as representatives, since they are obviously different in molecular orientation but nearly the same in domain size and interfacial width. We termed these nanostructures treated with $\mathbf{E_{treat}}$=0, $\mathbf{E_{treat}}$=-10 and $\mathbf{E_{treat}}$=10 as **SPE** (structures with block copolymers parallel to the electrodes), **SDC** (structures with free ends of donor blocks point towards the cathode) and **SDA** (structures with free ends of donor blocks point towards the anode) nanostructures, respectively. By solving the extended drift-diffusion equations, we obtained *J-V* (current density - applied voltage) curves for these representative nanostructures. In the calculations, most of the input parameters are typical for polymeric materials used in polymer photovoltaic cells. [11, 39, 41, 42] The anisotropic transport characteristic parameters of electron, hole and exciton mobility were set to 50, which is a moderate value chosen according to the reported values obtained in experiments.[43-45] Figure 3 shows the *J-V* curves for these representative nanostructures with applied voltages varying from 0 to 1.3 V. With the variation in the molecular orientation, the photovoltaic performance of these self-assembled nanostructures undergoes distinct changes. According to the *J-V* curves, we calculated the photovoltaic properties, *i.e.*, the power conversion efficiency *PCE*, short-circuit current density *Jsc*, open-circuit voltage *Voc* and fill factors *FF*, which are listed in Table 1. The *Voc* values in these self-assembled nanostructures with and without external field treatment are comparable. In contrast to the *Voc*, the *Jsc*, *FF* and *PCE* of the field-treated nanostructures (**SDC** and **SDA**) are significantly superior to those of the nanostructure without external field treatment (**SPE**). Additionally, the values of *Jsc*, *FF* and *PCE* of **SDA** are much higher than those of **SDC**. These results indicate that molecular orientation plays a critical role in the improvement in the photovoltaic performance of the self-assembled nanostructures. Among the nanostructures with various molecular orientations of the block copolymers, the **SDA** structure, with the free ends of the donor and acceptor blocks pointing towards the anode and cathode respectively, performs better than the others. Notably, in comparison with that of the **SPE** structure without external field treatment, the *PCE* of the **SDA** structure with external field treatment is improved by more than 150%. We also examined the photovoltaic performance of self-assembled nanostructures treated with a series of different external fields ($\mathbf{E_{treat}}$=-15~15). It was found that most of the nanostructures obtained with field treatment perform better than the **SPE** structure.

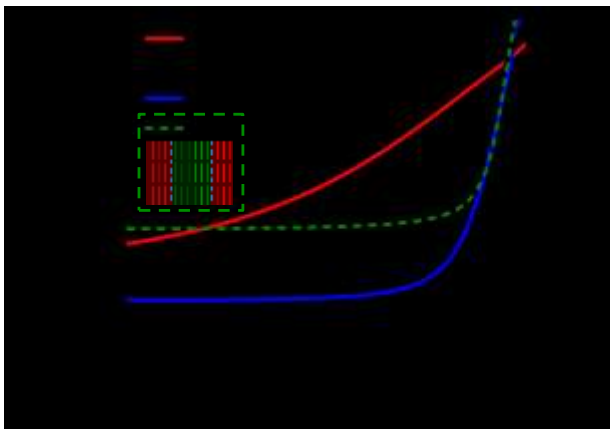

Figure 3 J-V curves for nanostructures (**SPE**, **SDC**, **SDA** and **SPA** (ideal)) with various molecular orientations self-assembled from block copolymers. The insert shows the ideal nanostructure (**SPA**) with donor molecules parallel to the D/A interface for comparison with nanostructures obtained from DPD simulations. In the insert, the red and green regions represent the acceptor and donor phases, respectively.

Table 1 Photovoltaic properties of **SPE**, **SDC**, **SDA** and **SPA** nanostructures with anisotropic transport parameter set to 25.

Nanostructures	Jsc (mA/cm^2)	Voc (V)	FF (%)	PCE (%)
SPE	11.7	1.24	35.4	5.23
SDC	14.1	1.25	44.6	7.75
SDA	15.5	1.24	71.8	13.9
SPA	10.8	1.23	77.1	10.4

To further confirm the performance advantage of the **SDA** structure, we also compared its photovoltaic properties with that of an ideal nanostructure. We constructed a nanostructure representing an ideal case for the phase-separated morphologies achieved in blends of donor and acceptors. The ideal nanostructure is also a lamellar structure (see the insert in Figure 3). The backbones of donor and acceptor molecules in the ideal nanostructure are assumed to be parallel to the D/A interfaces. We termed the ideal nanostructure as **SPA** (structures with donor and acceptor molecules parallel to the D/A interfaces). The *J-V* curve and photovoltaic properties of **SPA** nanostructure are also provided in Figure 3 and Table 1. The **SPA** structure exhibits a higher value of *FF* than the other structures, but the value of *Jsc* for **SPA** is lower. As a result, the photovoltaic performance of **SPA** is also lower than that of **SDA**.

The performance of polymer solar cells is dependent not only on molecular orientation but also on anisotropic transport characteristic of the charge carriers and excitons in the conjugated polymers. Therefore, we further examined the dependence of the photovoltaic properties on the anisotropic transport parameters (C_A) in the above four nanostructures. Figure 4 shows the photovoltaic properties against C_A in these

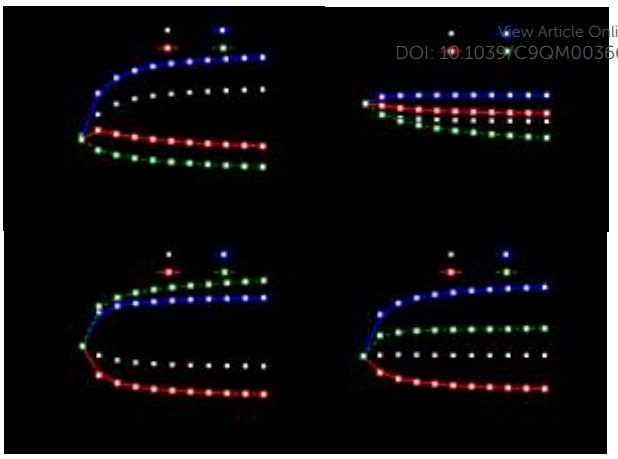

Figure 4 Plots of Jsc (a), Voc (b), FF (c) and PCE (d) against anisotropic transport parameter (C_A) for the **SPE**, **SDC**, **SDA** and **SPA** nanostructures.

nanostructures. The impact of molecular orientation on the photovoltaic performance is strongly dependent on the anisotropic transport parameter. In Figure 4a we observe that, for the isotropic block copolymers with C_A=0, all four nanostructures exhibit a similar *Jsc*. The similar *Jsc* values among these structures indicate that the molecular orientation cannot affect the photovoltaic performance when C_A=0. With increasing C_A, the difference in the *Jsc*s among these nanostructures becomes more obvious. The *Jsc* of **SDA** remains the highest. Compared with *Jsc*, *Voc* is less sensitive to the variation in C_A, as shown in Figure 4b. The differences in *FF* and PCE also become more obvious with the increase in C_A. These results indicate that the difference in the performance caused by the distinct molecular orientation among these nanostructures is strongly dependent on the anisotropic transport characteristic.

2.2 Mechanism underlying Photovoltaic Performance Enhancement

The mechanism underlying the enhancement in photovoltaic performance is related to the photovoltaic processes, which can be revealed by analyzing the equilibrium distributions of the exciton concentrations, photogenerated current densities and charge recombination rates. Figure 5a shows the one-dimensional distribution of excitons in the **SPE**, **SDC**, **SDA** and **SPA** structures. As shown in the figure, the exciton concentrations drop to very low values near the D/A interfaces, since the excitons dissociate in these regions. Among these four structures, we found that the exciton concentrations in **SPE**, **SDC** and **SDA** are much lower than those in the **SPA** structure, which means that more excitons in **SPE**, **SDC** and **SDA** can diffuse to the D/A interfaces. As more excitons diffuse to the D/A interfaces, the exciton dissociation rates (generation rates of charge carriers) in **SPE**, **SDC** and **SDA** are higher than those in **SPA**. These results suggest that the molecules perpendicular to the D/A interfaces (as in **SPE**) favor the diffusion of the excitons to the D/A interfaces and then the generation of charge carriers. In the **SDA** and **SDC** structures

where the free ends of the donor blocks respectively point towards the anode and cathode, the molecular orientation of the block copolymers is also beneficial for exciton diffusion and dissociation.

Figure 5b and c shows the hole-current density (Jp_y) and electron-current density (Jn_y) along the y-direction perpendicular to the electrodes in the **SDA**, **SDC**, **SPE** and **SPA** nanostructures. In the **SPE** and **SDC** structures, most holes and electrons transporting to the electrodes are near the D/A interfaces. These charge carriers near the D/A interface in these two structures are more likely to recombine with the opposite charge carriers, leading to a higher recombination rate (see Figure 5d). In the **SPA** structure, since the charge carrier mobility along the y-direction is very high, the charge carriers rapidly transport to the anodes. With rapid transport of the charge carriers, a higher posibility of recombination of holes and electrons can be avoided, resulting in a lower recombination rate in **SPA** than in **SPE** and **SDC**. Contrary to the distribution of Jp_y and Jn_y in **SPA**, **SPE** and **SDC**, the Jp_y and Jn_y in the center of the donor-rich and acceptor-rich domains in **SDA** is much higher than those along the D/A interfaces, which indicates that most holes and electrons concentrate in the center of the donor-rich and acceptor-rich domains and then transport to the anode and cathode, respectively. As a consequence, the recombination rates in **SDA** are significantly lower than those in the other three nanostructures.

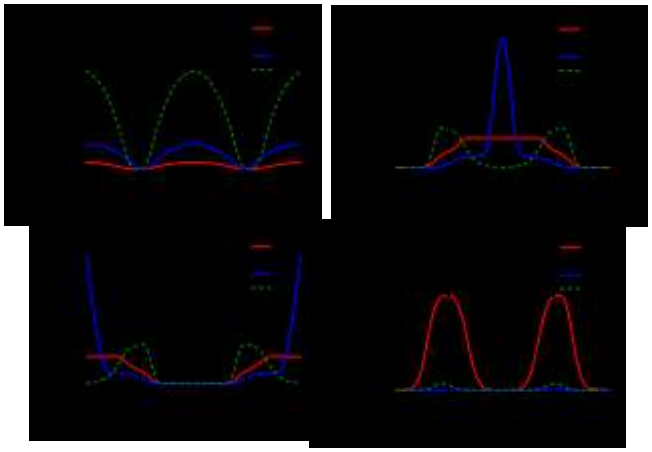

Figure 5 Plots of exciton density (a), hole-current density (b) and electron-current density along y-direction perpendicular to the electrodes (c), and charge carrier recombination rate (d) against the x-direction perpendicular to the D/A interface in the middle of the systems with the **SPE**, **SDC**, **SDA** and **SPA** structures. The black dashed lines in each figure are drawn to indicate where the D/A interfaces are located.

The performance enhancement mechanism for the **SDA** structure can be further understood by referring to the cartoon in Figure 6. In the **SPE**, **SDC** and **SDA** structures, there are projection components of block copolymers on the vector normal to the D/A interface. The mobility of excitons along the polymer backbone is higher than that in the direction perpendicular to the backbone. Therefore, the projections of block copolymers on the vector normal to the D/A interface in the **SPE**, **SDC** and **SDA** structures make the excitons diffuse faster to the interface and then avoid decay. The faster diffusion of excitons to the D/A interface results in lower exciton concentrations in the donor-rich domains and higher charge generation rates near the interfaces of the **SPE**, **SDC** and **SDA** structures than the **SPA** structure (see Figure 5a).

For the charge carriers (holes and electrons), the mobility along the polymer backbone is also higher than that in the direction perpendicular to the backbone. Therefore, in the **SDC**, **SDA** and **SPA** structures, the block copolymers with projections perpendicular to the electrodes can favor the transport of charge carriers to the electrodes, as illustrated in Figure 6b. However, since the free ends of the donor and acceptor blocks in the **SDC** structures point towards the wrong electrodes, the charge carriers have a tendency to flux back to the D/A interface and go into recombination with the opposite charge carriers. This behavior results in higher recombination rates in the **SDC** structure (see Figure 5d). Consequently, only the **SDA** and **SPA** structures enhance the transport of the charge carriers to the anodes. The above results indicate that, while the **SPE**, **SDC** and **SPA** structures can enhance either the generation or extraction of charge carriers, the **SDA** structure enhances both of these processes simultaneously. The simultaneous enhancement in charge generation and extraction results in the higher values of *Jsc* and *FF* in the **SDA** structure. Eventually, the **SDA** structure exhibits the best photovoltaic performance among these nanostructures.

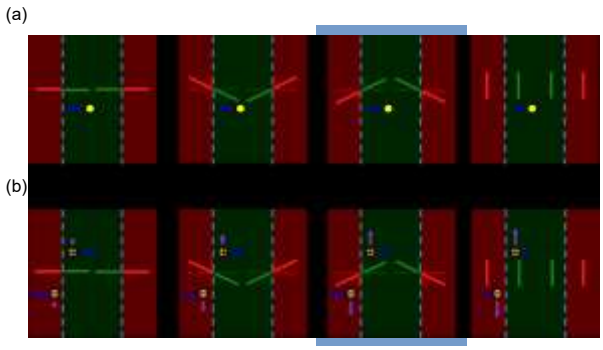

Figure 6 Schematic illustrations of diffusion and transport vector for the excitons (a), holes and electrons (b) in the **SPE**, **SDC**, **SDA** and **SPA** structures, respectively.

2.3 Effect of Variations in Parameters on Performance Enhancement

Although the molecular orientation has been shown to have a critical influence on the photovoltaic performance of nanostructures self-assembled from donor-acceptor diblock copolymers, demonstrations of structure-property relationships in polymer photovoltaics are often limited to one kind of material and cannot be applied universally across material systems. To confirm the generality of our findings, we compare the photovoltaic performances among the **SPA**, **SPE**, **SDA** and **SDC** structures with alterations in some important parameters such as the mobility of charge carriers and the diffusion length of excitons. Both the charge carrier mobility and the exciton diffusion length significantly affect the photovoltaic performance.[46]

The effect of the isotropic mobility of charge carriers was also studied. As shown in Figure 7a, with the increase in mobility, the *Jsc* value in the **SDA** is always higher than that in the other structures. The *Jsc*s in the **SDC** and **SPE** structures are sensitive to the changes in mobility. When the mobility is 10^{-10} $m^2V^{-1}s^{-1}$, the *Jsc*s in the **SDC** and **SPE** are much lower than that in **SDA**. As the mobility increases to a value larger than 10^{-7} $m^2V^{-1}s^{-1}$, the *Jsc*s increase to the value comparable to that in **SDA**. The *FF* values in **SDA** and **SPE** are always higher than those in **SDC** and **SPA** within the variation in mobility (see Figure 7b). With the higher values of *Jsc* and *FF*, **SDA** performs better than the other structures with various mobility, as shown in Figure 7c.

The effect of the exciton diffusion length on the performance of the four nanostructures was first investigated. As shown in Figure 7d, the *Jsc* values of the **SDA** and **SDC** nanostructures remain higher than those of the **SPA** and **SPE** nanostructures as the diffusion length of excitons increases from 4 nm to 24 nm. Figure 7e shows that the *FF* values of these four structures remain almost constant when the diffusion length is varied. Additionally, the *FF*s of **SDA** and **SPA** keep higher than those of the other two structures. With the *Jsc* and *FF* maintained at higher levels, **SDA** always exhibits the highest power conversion efficiency among the four systems with various exciton diffusion length (see Figure 7f).

The structural parameters, including the domain size and thickness of the active layer, can affect photovoltaic properties as well. We also compared the photovoltaic performances among the **SDA**, **SDC**, **SPA** and **SPE** structures with alterations in the domain size and thickness of the active layer (for details, see Figure S2). It was found that the **SDA** structure always exhibits higher values of the *Jsc* and *FF* and then performs much better than the other structures. As mentioned above, the finding that **SDA** performs better than the other structures is general over a large parameter space.

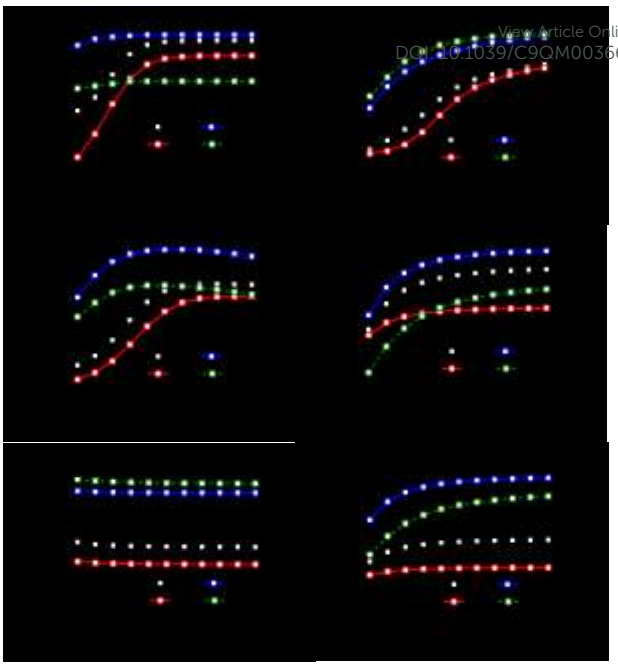

Figure 7 Plots of *Jsc* (a, d), *FF* (b, e) and *PCE* (c, f) against isotropic mobility of charge carriers and exciton diffusion length for the **SPE**, **SDC**, **SDA** and **SPA** nanostructures.

2.4 Comparison with Experiments

So far, there is no direct experimental study demonstrating the improved photovoltaic performance of block copolymers by modulating molecular orientation. However, our prediction can be supported by some experimental evidence from the works on polymer blend systems.[19, 24, 26, 29] External electric field treatment has been applied to modulate the molecular orientation of polymer blend solar cells and improved photovoltaic performance was obtained.[26, 27] For example, Solanki et al. applied external electric field to treat the self-organization of conjugated polymers containning P3HT (Poly(3-hexylthiophene)) and P3BT (poly(3-butylthiophene)) in polymer solar cells. [26] When an external E-field is applied during thermal annealing of the films, thiophene molecules get polarized and the polymer chains in the amorphous region align themselves with E-field. As the vertical ordering of the polymer chains increases, the Jsc and FF are enhanced and the power conversion efficiency is improved. In our simulations, we also observed that the block copolymers align themselves with E-field and the vertical ordering of polymer chains in **SDA** and **SDC** structures increased when external fields were applied. The power conversion efficiencies of **SDA** and **SDC** structures are found to be much higher than that for the general ones (**SPE**) without external field treatment. This result is qualitatively consistent with the experimental observations.

The finding about the high values of FF of **SPA** structure in our simulations can be supported by some experimental works. We observed in the simulations that for a **SPA** nanostructure with molecules parallel to the D/A interfaces, the charge carriers transport rapidly to the electrodes and therefore the

recombination rate is low. The rapid transport and low recombination of charge carriers lead to a high FF. In experiments, Yang et al. have obtained high FF via modulating molecular orientation in the nanoimprinted polymer solar cells.[47] They found that the molecular orientation could be altered from parallel to vertical alignment along the D/A interfaces by either narrowing the width or increasing the height of a P3HT nanograting. In the nanostructure with the narrowest and highest nanogratings, the P3HT molecules which are parallel to the D/A interface are in vertical alignment, similar to the ideal **SPA** nanostructure in our simulations. They observed that the nanoimprinted structures with the backbones of P3HT parallel to the D/A interfaces exhibit high FF, which is similar to the simulation results.

Modulating molecular orientation could be an effective way to enhance the photovoltaic performance in both polymer blend and block copolymer self-assembly systems. However, it should be noted that there are substantial differences between them. In polymer blend systems, modulation of molecular orientation is inevitably associated with changes in some structural factors such as phase purity and characteristic size. The inability to decouple these structural factors makes it a challenge to directly correlate molecular orientation with device performance. Additionally, the nanostructures formed in polymer blends are not well controlled and are prone to further macrophase-separate. Thus, the photovoltaic performance of polymer blend systems with modulated molecular orientation is not well repeatable and degrades with time. Block copolymers, which can form highly ordered and stable nanostructures with controllable molecular orientation, can overcome the shortcomings noted in the context of blend systems. External fields, including magnetic fields and electric fields, have been extensively utilized to control the molecular orientation and microdomain orientation of the block copolymer nanostructures.[30, 48-50] For example, Tao *et al.* demonstrated that the molecular orientation of poly-(2,5-di(2-ethylhexyloxy)-1,4-phenylenevinylene-*block*-1,4-isoprene) block copolymers can be modulated by coupling the magnetic field to the diamagnetic moment of individual conjugated blocks.[30] These works indicate that the high-efficiency block-copolymer system designed here could be realized by applying external fields to modulate the molecular orientation.

In this work, to the best of our knowledge, we provide the first indication that the photovoltaic performance of nanostructures formed by block copolymers can be improved markedly by modulating the molecular orientation. Applying external fields during the self-assembly process is proved to be an effective way to regulate the molecular orientation in block-copolymer-based solar cells. Interestingly, we found that the self-assembled nanostructures with external field treatment performed much better than the ones without treatment. This conclusion is general over a wide range of electronic parameters and structural parameters. Our simulation results show qualitative consistency with experimental evidence.

3. Conclusions

The multi-scale approach coupling DPD with a drift-diffusion model is extended to investigate the photovoltaic properties of nanostructures self-assembled from donor-acceptor diblock copolymers with various molecular orientations. We modulated the molecular orientation in the self-assembled nanostructures by applying external electric fields. Among the self-assembled nanostructures, the ones with the free ends of the donor and acceptor blocks respectively pointing towards the anode and cathode exhibit the highest efficiency with high *Jsc* and *FF*. This high efficiency is a result of the simultaneous enhancement in the generation and collection of charge carriers. Our simulation results could pave the way for preparing efficient block-copolymer-based photovoltaic devices by modulating molecular orientation.

4. Method

In our previous work,[34] we proposed a multi-scale approach coupling the DPD simulations with a drift-diffusion model to study the relationship between the photovoltaic properties and the self-assembled morphologies of block copolymers. The DPD method was conducted for determining the morphologies, while the drift-diffusion equations were solved for the photovoltaic properties. Here, to study the effect of molecular orientation on the photovoltaic performance of block copolymer films, we extended this multi-scale approach by introducing an external electric field into the DPD simulations and considering the anisotropic transport characteristics in the drift-diffusion model.

Mesoscopic simulations based on the DPD are performed to investigate the self-assembled morphologies.[51-54] DPD is a powerful tool that can be used for modeling physical phenomena occurring at larger time and length scales than typical molecular dynamics (MD). In the DPD method, a coarse-grained bead (DPD bead) represents a cluster of atoms. The evolution of the DPD beads is described by Newton's equations of motion. Newton's equations of motion for all bead positions and velocities are integrated by a modified velocity-Verlet algorithm. The force acting on a DPD bead α, $\mathbf{f}_\alpha$, includes the conservative force ($\mathbf{F}^{C}_{\alpha\beta}$), dissipative force ($\mathbf{F}^{D}_{\alpha\beta}$), and random force ($\mathbf{F}^{R}_{\alpha\beta}$). It is given by[51]

$$\mathbf{f}_\alpha=\sum_{\beta\neq\alpha}(\mathbf{F}^{C}_{\alpha\beta}+\mathbf{F}^{D}_{\alpha\beta}+\mathbf{F}^{R}_{\alpha\beta}) \quad (1)$$

More details of the DPD simulation method can be found in Section 1 of the Supporting Information.

In the DPD simulations, we consider a series of diblock copolymers consisting of donor and acceptor blocks. The neighboring beads in the copolymers are connected by spring bonds. The bonds are represented by a harmonic spring potential

$$U_{\alpha\beta}=K_b(1-r_{\alpha\beta}/r_{eq})^2 \quad (2)$$

where the spring constant and the equilibrium bond distance are set to K_b =50 and r_{eq}=0.5, respectively. Since most semiconductor polymers are rigid, we include a three-body stiffness potential along the copolymer with the form

$$U_{angle}=K_a(\cos\theta-\cos\theta_0)^2 \quad (3)$$

where K_a= 20 and θ_0=π.

In the DPD simulations, external fields are applied to modulate the molecular orientation through the interaction between the external field and donor blocks.[55] The interaction between the donor blocks and external fields is modeled by coupling the unit vector $\mathbf{P}_i$ along the long axis of the *i*th donor block to an external field $\mathbf{E}_{treat}$ pointing along the z-axis (the axis perpendicular to the electrodes) through the interaction potential

$$U_{control}=\mathbf{E}_{treat}\mathbf{P}_i \quad (4)$$

Within the interaction, a torque was applied to rotate the block copolymers towards alignment with the direction of $\mathbf{E}_{treat}$. The polymer blocks with a net dipole moment along the long axis of the donor block were constructed according to the work reported by Solanki et al..[26, 56] They found that the direction of the intrinsic dipole moment in Poly(3-hexylthiophene) (P3HT) and poly(3-butylthiophene) (P3BT) is along the polymer chain, by analyzing the electrostatic potential distribution in the monomer of these donor polymers.[26] Their works indicate that the model of block copolymers with donor blocks having a net dipole moment along the long axis is realistic. The model of block copolymers with donor blocks with dipole moments along the long axis is based on experiments.

In the DPD simulation boxes, NVT ensemble and periodic boundary conditions are adopted. The particle density ρ is set to 4. The interaction strengths a_{ij} between DPD beads of same type are given by a_{DD} = a_{AA} = 20, where D and A stand for the beads in the donor and acceptor blocks, respectively. The interaction strengths a_{ij} ($i\neq j$) between DPD beads of different types are set to 70. The friction coefficient γ and the noise amplitude σ are respectively set to 4.5 and 3.0, and thus k_BT = 1.0. In this work, more than 2×10^7 DPD steps are performed so that the computing time is long enough for the system to achieve an equilibrium state. To establish a correlation between simulation parameters and experimental values and thus establish a physical length scale in our system, we equate the thickness of a lamellar domain obtained from DPD for the D_4A_4 diblock without external field treatment to 10 nm.[11, 30]

After obtaining the self-assembled nanostructures *via* DPD simulation, we calculate the photovoltaic properties of these nanostructures by solving the drift-diffusion equations involving the electric potential ψ[V] and the charge carrier number densities *e*, *h*, and *X* [m^{-3}] of electrons, holes and excitons, respectively.[31, 57] The current densities of the holes and electrons are calculated using the forms[58]

$$\mathbf{J}_e=-\boldsymbol{\mu}(\mathbf{r})e(\mathbf{r})\nabla\psi(\mathbf{r})-\boldsymbol{D}_e(r)\nabla e(\mathbf{r}) \quad (5)$$
$$\mathbf{J}_h=\boldsymbol{\mu}(\mathbf{r})h(\mathbf{r})\nabla\psi(\mathbf{r})-\boldsymbol{D}_e(\mathbf{r})\nabla h(\mathbf{r}) \quad (6)$$

The total current density $\mathbf{J}$ is the summation of $\mathbf{J}_e$ and $\mathbf{J}_h$. More details of the drift-diffusion model are shown in Section 2 of the Supporting Information. The drift-diffusion equations in the drift-diffusion model are numerically solved by the finite difference method.

In the extended drift-diffusion model, we account for the anisotropic nature of transport both in the donor and acceptor phases by describing the mobilities of the charge carriers and excitons as anisotropic mobility tensors. The mobility tensors were determined by the molecular orientation:

$$\boldsymbol{\mu}_m(\mathbf{r})=\left(\mu_{m||}(\mathbf{r})-\mu_{m\perp}(\mathbf{r})\right)\hat{\mathbf{v}}\hat{\mathbf{v}}+\mu_{m\perp}(\mathbf{r})\mathbf{I} \quad (m=e,h,\text{or } X) \quad (7)$$

where $\hat{\mathbf{v}}$ is the local nematic director (director of backbones of block copolymers), and $\mu_{m||}$ and $\mu_{m\perp}$ are the mobilities in the directions parallel and perpendicular to the local nematic director, respectively. $\mathbf{I}$ is the identity matrix. $\mu_{m||}$ and $\mu_{m\perp}$ were determined by the local orientational order parameter $S(\mathbf{r})$:[33]

$$\begin{cases}\mu_{m||}(\mathbf{r})=\mu_{m,iso}+\frac{2\mu_{m,ani}S(\mathbf{r})}{3}=\frac{(\mu_{m||,S=1}+2\mu_{m\perp,S=1})}{3}+\frac{2(\mu_{m||,S=1}-\mu_{m\perp,S=1})S(\mathbf{r})}{3}\\ \mu_{m\perp}(\mathbf{r})=\mu_{m,iso}-\frac{\mu_{m,ani}S(\mathbf{r})}{3}=\frac{(\mu_{m||,S=1}+2\mu_{m\perp,S=1})}{3}-\frac{(\mu_{m||,S=1}-\mu_{m\perp,S=1})S(\mathbf{r})}{3}\end{cases} \quad (8)$$

where $\mu_{m,\,iso}$ and $\mu_{m,\,ani}$ are the isotropic and anisotropic contributions to the mobilities, respectively, and $\mu_{m||,S=1}$ and $\mu_{m\perp,S=1}$ are the mobilities in the directions parallel and perpendicular to the backbones of block copolymers, respectively.

The output of the DPD simulations serves as the input to estimate the local dielectric constants and mobility constants at the centre of mesh cells in the finite difference method for the drift-diffusion equations. The total dielectric constants $\varepsilon(\mathbf{r})$ and mobility constants $\boldsymbol{\mu}(\mathbf{r})$ at each point are obtained by linearly weighting the contributions of the different components based on the respective volume fractions, *i.e.*,

$$\varepsilon(\mathbf{r})=\sum_i\varphi_i(\mathbf{r})\varepsilon_i \quad (9)$$
$$\boldsymbol{\mu}(\mathbf{r})=\sum_i\varphi_i(\mathbf{r})\boldsymbol{\mu}_i \quad (10)$$

where $\boldsymbol{\varepsilon}_i$ and $\boldsymbol{\mu}_i$ denote the permittivity and mobility constant of component *i*, and $\varphi_i(\mathbf{r})$ refers to the volume fraction of component *i* at $\mathbf{r}$.

The electrical parameters used in the photovoltaic calculations are listed in Table S1. Most of the parameters are typical values of polymeric materials used in polymer photovoltaic cells.[11, 39, 41, 42, 59] The energy levels of the acceptor and donor are taken from reference.[11] The LUMO energy level of the acceptor is taken to be 3.5 eV, and the HOMO energy level of the donor is taken to be 4.9 eV. Both the electron and the isotropic parts of the hole mobilities are set to 5×10^{-9} $m^{-2}V^{-1}s^{-1}$, which is near the magnitude of the charge mobilities of P3HT (poly(3-hexylthiophene)) and PFTBT (poly-((9,9-dioctylfluorene)-2,7-diyl-alt-[4,7-bis(thiophen-5-yl)-2,1,3-benzothiadiazole]-2′,2″-diyl)).

Conflicts of interest

There are no conflicts to declare.

Acknowledgements

This work was supported by the National Natural Science Foundation of China (21774032, 51833003 and 51621002). Support from Project of Shanghai Municipality (16520721900) is also appreciated.

References

1. T. Kim, J.-H. Kim, T. E. Kang, C. Lee, H. Kang, M. Shin, C. Wang, B. Ma, U. Jeong, T.-S. Kim and B. J. Kim, *Nat. Commun.*, 2015, **6**, 8547.
2. W. Cai, X. Gong and Y. Cao, *Sol. Energy Mater. Sol. Cells*, 2010, **94**, 114-127.
3. M. Zhang, W. Gao, F. Zhang, Y. Mi, W. Wang, Q. An, J. Wang, X. Ma, J. Miao, Z. Hu, X. Liu, J. Zhang and C. Yang, *Energy Environ. Sci.*, 2018, **11**, 841-849.
4. S. Zhang, Y. Qin, J. Zhu and J. Hou, *Adv. Mater.*, 2018, **30**, 1800868.
5. F. Zhao, S. Dai, Y. Wu, Q. Zhang, J. Wang, L. Jiang, Q. Ling, Z. Wei, W. Ma, W. You, C. Wang and X. Zhan, *Adv. Mater.*, 2017, **29**, 1700144.
6. L. Meng, Y. Zhang, X. Wan, C. Li, X. Zhang, Y. Wang, X. Ke, Z. Xiao, L. Ding, R. Xia, H.-L. Yip, Y. Cao and Y. Chen, *Science*, 2018, **361**, 1094-1098.
7. H. Li, Z. Xiao, L. Ding and J. Wang, *Sci. Bull.*, 2018, **63**, 340-342.
8. J. Yuan, Y. Zhang, L. Zhou, G. Zhang, H.-L. Yip, T.-K. Lau, X. Lu, C. Zhu, H. Peng, P. A. Johnson, M. Leclerc, Y. Cao, J. Ulanski, Y. Li and Y. Zou, *Joule*, 2019, **3**, 1.
9. M. An, F. Xie, X. Geng, J. Zhang, J. Jiang, Z. Lei, D. He, Z. Xiao and L. Ding, *Adv. Energy Mater.*, 2017, **7**, 1602509.
10. C. Guo, Y. Lee, Y.-H. Lin, J. Strzalka, C. Wang, A. Hexemer, C. Jaye, D. A. Fischer, R. Verduzco, Q. Wang and E. D. Gomez, *Macromolecules*, 2016, **49**, 4599-4608.
11. C. Guo, Y.-H. Lin, M. D. Witman, K. A. Smith, C. Wang, A. Hexemer, J. Strzalka, E. D. Gomez and R. Verduzco, *Nano Letters*, 2013, **13**, 2957-2963.
12. Y. Lee and E. D. Gomez, *Macromolecules*, 2015, **48**, 7385-7395.
13. V. D. Mitchell and D. J. Jones, *Polym. Chem.*, 2018, **9**, 795-814.
14. J. H. Lee, C. G. Park, A. Kim, H. J. Kim, Y. Kim, S. Park, M. J. Cho and D. H. Choi, *ACS Appl. Mater. Interfaces*, 2018, **10**, 18974-18983.
15. G. Li, R. Zhu and Y. Yang, *Nat. Photonics*, 2012, **6**, 153.
16. W. Ma, J. R. Tumbleston, M. Wang, E. Gann, F. Huang and H. Ade, *Adv. Energy Mater.*, 2013, **3**, 864-872.
17. B. Huang, J. A. Amonoo, A. Li, X. C. Chen and P. F. Green, *J Phys. Chem. C*, 2014, **118**, 3968-3975.
18. S. Venkatesan, J. Chen, E. C. Ngo, A. Dubey, D. Khatiwada, C. Zhang and Q. Qiao, *Nano Energy*, 2015, **12**, 457-467.
19. J. R. Tumbleston, B. A. Collins, L. Yang, A. C. Stuart, E. Gann, W. Ma, W. You and H. Ade, *Nat. Photonics*, 2014, **8**, 385.
20. J.-L. Brédas and R. Silbey, *Science*, 2009, **323**, 348.
21. B. O'Connor, R. J. Kline, B. R. Conrad, L. J. Richter, D. Gundlach, M. F. Toney and D. M. DeLongchamp, *Adv. Funct. Mater.*, 2011, **21**, 3697-3705.
22. V. Skrypnychuk, G.-J. A. H. Wetzelaer, P. I. Gordiichuk, S. C. B. Mannsfeld, A. Herrmann, M. F. Toney and D. R. Barbero, *Adv. Mater.*, 2016, **28**, 2359-2366.
23. J. W. Jo, J. W. Jung, H. Ahn, M. J. Ko, A. K. Y. Jen and H. J. Son, *Adv. Energy Mater.*, 2016, **7**, 1601365.
24. Z. Luo, C. Sun, S. Chen, Z.-G. Zhang, K. Wu, B. Qiu, C. Yang, Y. Li and C. Yang, *Adv. Energy Mater.*, 2018, **8**, 1800856.
25. T. Kumari, S. M. Lee, S.-H. Kang, S. Chen and C. Yang, *Energy Environ. Sci.*, 2017, **10**, 258-265. View Article Online DOI: 10.1039/C9QM00366E
26. A. Solanki, A. Bagui, G. Long, B. Wu, T. Salim, Y. Chen, Y. M. Lam and T. C. Sum, *ACS Appl. Mater. Interfaces*, 2016, **8**, 32282.
27. C.-C. Lin, Y.-Y. Lin, S.-S. Li, C.-C. Yu, C.-L. Huang, S.-H. Lee, C.-H. Du, J.-J. Lee, H.-L. Chen and C.-W. Chen, *Energy Environ. Sci.*, 2011, **4**, 2134-2139.
28. A. Solanki, B. Wu, T. Salim, E. K. L. Yeow, Y. M. Lam and T. C. Sum, *J Phys. Chem. C*, 2014, **118**, 11285-11291.
29. J. Jung, W. Lee, C. Lee, H. Ahn and B. J. Kim, *Adv. Energy Mater.*, 2016, **6**, 1600504.
30. Y. Tao, H. Zohar, B. D. Olsen and R. A. Segalman, *Nano Lett.*, 2007, **7**, 2742-2746.
31. G. A. Buxton and N. Clarke, *Phys. Rev. B*, 2006, **74**, 085207.
32. A. Pershin, S. Donets and S. A. Baeurle, *Polymer*, 2014, **55**, 1507-1513.
33. M. Shah and V. Ganesan, *Macromolecules*, 2010, **43**, 543-552.
34. Z. Xu, J. Lin, L. Zhang, L. Wang, G. Wang, X. Tian and T. Jiang, *ACS Appl. Mater. Interfaces*, 2018, **10**, 22552-22561.
35. Z. Xu, J. Lin, Q. Zhang, L. Wang and X. Tian, *Polym. Chem.*, 2016, **7**, 3783-3811.
36. B. P. Lyons, N. Clarke and C. Groves, *Energy Environ. Sci.*, 2012, **5**, 7657-7663.
37. L. J. A. Koster, O. Stenzel, S. D. Oosterhout, M. M. Wienk, V. Schmidt and R. A. J. Janssen, *Adv. Energy Mater.*, 2013, **3**, 615-621.
38. T. Kirchartz and J. Nelson, in *Multiscale Modelling of Organic and Hybrid Photovoltaics*, eds. D. Beljonne and J. Cornil, Springer-Verlag, Berlin Heidelberg, 2014, pp. 279-324.
39. A. B. Gavin and C. Nigel, *Modell. Simul. Mater. Sci. Eng.*, 2007, **15**, 13.
40. H. Sirringhaus, P. J. Brown, R. H. Friend, M. M. Nielsen, K. Bechgaard, B. M. W. Langeveld-Voss, A. J. H. Spiering, R. A. J. Janssen, E. W. Meijer, P. Herwig and D. M. de Leeuw, *Nature*, 1999, **401**, 685.
41. M. Hufnagel, M. Fischer, T. Thurn-Albrecht and M. Thelakkat, *Macromolecules*, 2016, **49**, 1637-1647.
42. B. Ray, P. R. Nair and M. A. Alam, *Sol. Energy Mater. Sol. Cells*, 2011, **95**, 3287-3294.
43. J. F. Hulvat and S. I. Stupp, *Adv. Mater.*, 2004, **16**, 589-592.
44. K. Sakamoto, T. Yasuda, K. Miki, M. Chikamatsu and R. Azumi, *J. Appl. Phys.*, 2011, **109**, 013702.
45. I. O. Shklyarevskiy, P. Jonkheijm, N. Stutzmann, D. Wasserberg, H. J. Wondergem, P. C. M. Christianen, A. P. H. J. Schenning, D. M. de Leeuw, Ž. Tomović, J. Wu, K. Müllen and J. C. Maan, *J. Am. Chem. Soc.*, 2005, **127**, 16233-16237.
46. Y. Terao, H. Sasabe and C. Adachi, *Appl. Phys. Lett.*, 2007, **90**, 103515.
47. Y. Yang, K. Mielczarek, M. Aryal, A. Zakhidov and W. Hu, *Nanoscale*, 2014, **6**, 7576-7584.
48. M. Gopinadhan, Y. Choo, K. Kawabata, G. Kaufman, X. Feng, X. Di, Y. Rokhlenko, L. H. Mahajan, D. Ndaya, R. M. Kasi and C. O. Osuji, *Proc. Natl. Acad. Sci. U. S. A.*, 2017, **114**, E9437.
49. H. U. Jeon, H. M. Jin, J. Y. Kim, S. K. Cha, J. H. Mun, K. E. Lee, J. J. Oh, T. Yun, J. S. Kim and S. O. Kim, *Mol. Syst. Des. Eng.*, 2017, **2**, 560-566.
50. C. W. Pester, C. Liedel, M. Ruppel and A. Böker, *Prog. Polym. Sci.*, 2017, **64**, 182-214.
51. R. D. Groot and P. B. Warren, *J. Chem. Phys.*, 1997, **107**, 4423-4435.
52. R. D. Groot and T. J. Madden, *J. Chem. Phys.*, 1998, **108**, 8713-8724.

View Article Online
DOI: 10.1039/C9QM00366E

53. Q. Zhang, J. Lin, L. Wang and Z. Xu, *Prog. Polym. Sci.*, 2017, **75**, 1-30.
54. X. Liu, W. Gao, L. Wang, C. Zhang and J. Lin, *Acta Polym. Sin.*, 2018, 1279.
55. A. AlSunaidi, W. K. den Otter and J. H. R. Clarke, *J. Chem. Phys.*, 2013, **138**, 154904.
56. B. Xia, D. Bao, S. Upadhyayula, G. Jones and V. I. Vullev, *The Journal of Organic Chemistry*, 2013, **78**, 1994-2004.
57. D. Bartesaghi and L. J. A. Koster, *Adv. Funct. Mater.*, 2014, **25**, 2013-2023.
58. F. Monestier, J.-J. Simon, P. Torchio, L. Escoubas, F. Flory, S. Bailly, R. de Bettignies, S. Guillerez and C. Defranoux, *Sol. Energy Mater. Sol. Cells*, 2007, **91**, 405-410.
59. Y. Fu, J. Qu, Y. Geng, B. Wang, Y. Han and Z. Xie, *Org. Electron.*, 2018, **58**, 75-81.